Spike timing-dependent plasticity induces non-trivial topology in the brain

R. R. Borges[1,2], F. S. Borges[1], E. L. Lameu[1], A. M. Batista[1,3,4], K. C. Iarosz[4], I. L. Caldas[4], C. G. Antonopoulos[5], M. S. Baptista[6]

[1] *Pós-Graduação em Ciências, Universidade Estadual de Ponta Grossa, Ponta Grossa, PR, Brazil.*

[2] *Departamento de Matemática, Universidade Tecnológica Federal do Paraná, 86812-460, Apucarana, PR, Brazil.*

[3] *Departamento de Matemática e Estatística, Universidade Estadual de Ponta Grossa, Ponta Grossa, PR, Brazil.*

[4] *Instituto de Física, Universidade de São Paulo, São Paulo, SP, Brazil.*

[5] *Department of Mathematical Sciences, University of Essex, Wivenhoe Park, UK.*

[6] *Institute for Complex Systems and Mathematical Biology, Aberdeen, SUPA, UK.*

Abstract

We study the capacity of Hodgkin-Huxley neuron in a network to change temporarily or permanently their connections and behavior, the so called spike timing-dependent plasticity (STDP), as a function of their synchronous behavior. We consider STDP of excitatory and inhibitory synapses driven by Hebbian rules. We show that the final state of networks evolved by a STDP depend on the initial network configuration. Specifically, an initial all-to-all topology envolves to a complex topology. Moreover, external perturbations can induce co-existence of clusters, those whose neurons are synchronous and those whose neurons are desynchronous. This work reveals that STDP based on Hebbian rules leads to a change in the direction of the synapses between high and low frequency neurons, and therefore, Hebbian learning can be explained in terms of preferential attachment between these two diverse communities of neurons, those with low-frequency spiking neurons, and those with higher-frequency spiking neurons.

Keywords: plasticity, synchronization, network
PACS: 87.10Hk, 87.19.lj, 87.19.lw

1. Introduction

Neuroplasticity, also known as brain plasticity or brain malleability (Strong et al., 1998; Brenner et al., 2000), refers to the ability of the brain to reorganize neural pathways in response to new information, environment, development, sensory stimulation, or damage (Draganski et al., 2004; James, 1890; Lashley, 1923). The term neuroplasticity was firstly introduced in 1948 by neuroscientist J. Konorski in a work (Konorski, 1948) that showed the associative learning as a result of the adaptation of the brain to external stimuli. In 1949, D. O. Hebb, in his book entitled "The Organization of Behavior" (Hebb, 1949), proposed a plasticity rule, today known as Hebb's rule.

Scientific advances in neuroimaging and in noninvasive brain stimulation have provided insights to understand better neuroplasticity. Learning-induced structural alterations in gray and white matter have been documented in human brain (Dayan & Cohen, 2011). Draganski and collaborators (Draganski et al., 2004) used whole-brain magnetic-resonance imaging to observe learning-induced neuroplasticity. They verified structural changes in areas of the brain associated with the processing and storage of complex visual motion. Lu and collaborators (Lu et al., 2003) demonstrated that neuroplasticity is affected by environmental stimuli. In addition, neuroimaging studies have showed alterations of neuroplasticity in depression, namely depressive disorder may be associated with impairment of neuroplasticity (Fuchs et al., 2004).

Aiming at understanding the fundamental mechanisms behind plasticity, Popovych and collaborators studied the effect of noise on synchronous behavior in globally-coupled spiking Hodgkin-Huxley neurons with spike timing-dependent plasticity (STDP) and excitatory synapses (Popovych et al., 2013; Borges et al., 2016). STDP networks have nodes that adapt their synaptic strength according to some rule based on their spike timings (Gilson et al., 2010; Markram et al., 2011; Markram et al., 2012). Abarbanel and Talathi (Abarbanel & Talathi, 2006) studied a neural circuit responsible for recognizing interspike interval sequences by means of STDP of inhibitory synapses. Similar results, though using different kinds of neural models, have been reported earlier by Kalitzin and collaborators (Kalitzin et al., 2000), where it was shown that coherent input can enhance synapses inducing high connectivity, whereas mutually anti-correlated inputs to individual neurons wea-

*Corresponding author: antoniomarcosbatista@gmail.com

kens connectivity. On the contrary, the work in (Popovych et al., 2013) however shows that a fully uncorrelated input can enhance connectivity. Sadeh and collaborators (Sadeh et al., 2015) studied the emergence of functionally specific connectivity in the visual cortex with Hebbian plasticity based on visual experience. They showed that plasticity can lead to functionally specific and stable connections in random networks composed of leaky integrate-and-fire neurons. In our work, we focus the attention on the network dependence on plasticity. To do that, we consider an initial all-to-all topology and focus on the changes in synchronous and non synchronous states caused in a Hodgkin-Huxley neural network with excitatory (eSTDP) and inhibitory synapses (iSTDP).

Neural spike synchronization is responsible for information transfer (Antonopoulos et al., 2015; Baptista et al., 2016), and can be associated with forms of dysfunction. For instance, abnormally synchronized oscillatory activity has been reported in Parkinson's disease (Hammond et al., 2007), epilepsy (Uhlhaas & Singer, 2006) and some other neurological disorders. Synchronous behavior was analised in systems of synfire chains to solve binding problems. It was verified that dynamics of binding may be modeled by competitive synchronization among synfire chains (Abeles et al., 2004; Hayon & Lehmann, 2005). Moreover, synfire chains have been considered to describe information transfer phenomena and coherent spiking (Wang et al., 2016).

Our main goal is to show that spike timing-dependent plasticity of excitatory and inhibitory synapses induces non-trivial topologies in the plastic brain. Initial networks of neurons fully connected, evolve to a non trivial complex network. Consequently, this non-trivial topology alters the synchronous behavior. In our results, we have observed for some parameter conditions not only the improvement of neural spiking synchronization, but also for other parameter conditions that promote desynchronization. We have also observed concurrent synchronous and non synchronous behavior in the neurons of a network constructed for a particular set of parameters. Therefore, the onset of synchronicity comes along side with desynchronicity in the plastic brain. This balance between different synchronous behaviors is vital to maintain a fundamental property of a brain network. Clusters need to be sufficiently synchronous for information to be efficiently exchanged, but at the same time sufficiently desynchronous to behave independently. Finally, we show that when there is an external perturbation, the plastic neural network has an abrupt change in behavior characterized by a first-order transition.

This paper is organized as follows: In Section II we introduce the neural network described by coupled Hodgkin-Huxley neural model. In Section III, we discuss our results about neural synchronization considering eSTDP and iSTDP. In the last Section, we draw our conclusions.

2. Neural network

In this work, we focus on eSTDP and iSTDP based on Hebbian theory proposed in Ref. (Hebb, 1949). These plastic mechanisms consist of synapses that become stronger or weaker depending on the pre and postsynaptic neurons' activity. We have considered an initial network with a global coupling, with chemical synapses where the connections are unidirectional, and the local dynamics is described by the Hodgkin-Huxley model (Izhikevich, 2004; Hodgkin & Huxley, 1952). The system is given by

$$\begin{aligned} C\dot{V}_i &= I_i - g_{\rm K} n_i^4 (V_i - E_{\rm K}) - g_{\rm Na} m_i^3 h_i (V_i - E_{\rm Na}) \\ &\quad - g_L (V_i - E_{\rm L}) + \frac{(V_r^{\rm Exc} - V_i)}{\omega_{\rm Exc}} \sum_{j=1}^{N_{\rm Exc}} \varepsilon_{ij} s_j \\ &\quad + \frac{(V_r^{\rm Inhib} - V_i)}{\omega_{\rm Inhib}} \sum_{j=1}^{N_{\rm Inhib}} \sigma_{ij} s_j + \Gamma_i, \qquad (1) \\ \dot{n}_i &= \alpha_{n_i}(V_i)(1 - n_i) - \beta_{n_i}(V_i) n_i, \qquad (2) \\ \dot{m}_i &= \alpha_{m_i}(V_i)(1 - m_i) - \beta_{m_i}(V_i) m_i, \qquad (3) \\ \dot{h}_i &= \alpha_{h_i}(V_i)(1 - h_i) - \beta_{h_i}(V_i) h_i, \qquad (4) \end{aligned}$$

where C is the membrane capacitance (μF/cm^2), V_i is the membrane potential (mV) of neuron i ($i = 1, ..., N$), I_i is a constant current density randomly distributed in the interval $[9.0, 10.0]$, $\omega_{\rm Exc}$ (excitatory) and $\omega_{\rm Inhib}$ (inhibitory) are the average degree connectivities, ε_{ij} and σ_{ij} are the excitatory and inhibitory coupling strengths from the presynaptic neuron j to the postsynaptic neuron i (Gray, 1959). The ε_{ij} values are in the interval $[0, 0.5]$ and the σ_{ij} values are in the interval $[0, 2\sigma_M]$. In our simulations, the maximum value for ε_{ij} is equal to 0.5 according to Reference (Popovych et al., 2013), and we consider the maximum value for σ_M equal to 0.75 due to the fact that for $\sigma_{ij} < 1.5$ we observe a transition from synchronized to desynchronized states. In addition, we have discarded a transient of 1.95×10^6ms. We consider that 80% of the neurons are excitatorily coupled ($N_{\rm Exc}$) and 20% of them are inhibitorily coupled ($N_{\rm Inhib}$) according to anatomical estimates for the neocortex (Noback et al., 2005). Both populations receive input from all other neurons in own population and from the other population. We also consider an external perturbation Γ_i, so that each neuron randomly chosen receives an input with a constant intensity $\gamma = 10\mu$A/cm^2 during 1ms. In each time step $t_{\rm step} = 0.01$ms a random input with amplitude γ is applied to each neuron with a probability equal to $t_{\rm step}/14$, where 14ms approximately corresponds to the inter-spike interval of the Hodgkin-Huxley neuron. Functions $m(V_i)$ and $n(V_i)$ represent the activation for sodium and potassium, respectively, and $h(V_i)$ is the function for the inactivation of sodium. Functions α_n, β_n, α_m, β_m, α_h, β_n are given by

$$\begin{aligned} \alpha_n(v) &= \frac{0.01v + 0.55}{1 - \exp(-0.1v - 5.5)}, \qquad (5) \\ \beta_n(v) &= 0.125 \exp\left(\frac{-v - 65}{80}\right), \qquad (6) \end{aligned}$$

$$\alpha_m(v) = \frac{0.1v+4}{1-\exp\left(-0.1v-4\right)}, \quad (7)$$

$$\beta_m(v) = 4\exp\left(\frac{-v-65}{18}\right), \quad (8)$$

$$\alpha_h(v) = 0.07\exp\left(\frac{-v-65}{20}\right), \quad (9)$$

$$\beta_h(v) = \frac{1}{1+\exp\left(-0.1v-3.5\right)}, \quad (10)$$

where $v = V/[mV]$. Parameter g is the conductance and E the reversal potentials for each ion. Depending on the value of the external current density I_i (μA/cm^2) the neuron can present single spike activity or periodic spikings. In the case of periodic spikes, if the constant I_i increases, the spiking frequency also increases. In this work, we consider $C = 1$ μF/cm^2, $E_{\rm Na} = 50$mV, $E_{\rm K} = -77$ mV, $E_{\rm L} = -54.4$ mV, $g_{\rm Na} = 120$ mS/cm^2, $g_{\rm K} = 36$ mS/cm^2, $g_{\rm L} = 0.3$ mS/cm^2. The neurons are excitatorily coupled with a reversal potential $V_r^{\rm Exc} = 20$mV, and inhibitorily coupled with a reversal potential $V_r^{\rm Inhib} = -75$mV. The presynaptic potential s_i is given by (Destexhe et al., 1994; Golomb & Rinzel, 1993)

$$\frac{ds_i}{dt} = \frac{5(1-s_i)}{1+\exp\left(-\frac{v_i+3}{8}\right)} - s_i, \quad (11)$$

where $v_i = V_i/[mV]$.

One of the key principles of behavioral neuroscience is that experience can modify the brain structure, what is known as neuroplasticity (Ramon Y Cajal, 1928). Although the idea that experience may modify the brain structure can probably be traced back to the 1890s (Bliss & Gardner-Medwin, 1973; Bliss & Collingridge, 1993), it was Hebb who made this a central feature in his neuropsychological theory (Hebb, 1961). With this in mind, we consider excitatory and inhibitory spike timing-dependent plasticity according to the Hebbian rule. The coupling strengths ε_{ij} and σ_{ij} are adjusted based on the relative timing between the spikes of presynaptic and postsynaptic neurons (Bi & Poo, 1998; Haas et al., 2006).

The plasticity dynamics can be mathematically defined as

$$\frac{d\Delta\varepsilon(t)}{dt} = f(\Delta\varepsilon, V, t), \quad (12)$$

where $\Delta\varepsilon$ is the update value of the synaptic weight. Kalitzin and collaborators (Kalitzin et al., 2000) considered a function f that depends on the activation of the synapse, the transmembrane potential of the postsynaptic neuron, and the thresholds for switching on long-term potentiation and the long-term depression (Artola et al., 1990). In this work, we consider a linear function f of the form $f(\Delta\varepsilon, t) = (a + c/t)\Delta\varepsilon$. The solution to the differential equation, Eq. (12), is given by $\Delta\varepsilon = bt^c\exp(at)$, where a, b and c are constants. For $c = 0$ and $c \neq 0$, eSTDP and iSTDP are obtained, respectively. The plasticity dynamics introduced by means of this linear function is not fundamentally related to physiological processes (Artola et al., 1990), but, by means of this function it is possible to find a fit that describes experimental results of eSTDP and iSTDP obtained in Refs. (Bi & Poo, 1998) and (Haas et al., 2006).

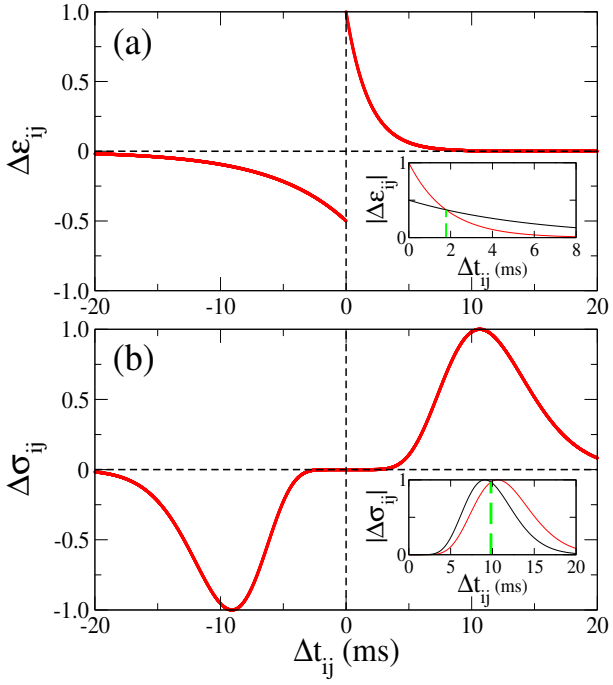

Figure 1: (Color online) Plasticity as a function of the difference of spike timing of post and presynaptic (a) excitatory (eSTDP) and (b) inhibitory (iSTDP) synapse. The insets show the absolute value of the plasticity function.

The excitatory eSTDP is given by

$$\Delta\varepsilon_{ij} = \begin{cases} A_1\exp(-\Delta t_{ij}/\tau_1)\ , & \Delta t_{ij} \geq 0 \\ -A_2\exp(\Delta t_{ij}/\tau_2)\ , & \Delta t_{ij} < 0 \end{cases}, \quad (13)$$

where $\Delta t_{ij} = t_i - t_j = t_{\rm pos} - t_{\rm pre}$, $t_{\rm pre}$ is the spike time of the presynaptic and $t_{\rm pos}$ the spike time of the postsynaptic neuron. Figure 1(a) exhibits the result obtained from Eq. (13) for $A_1 = 1.0$, $A_2 = 0.5$, $\tau_1 = 1.8$ms, and $\tau_2 = 6.0$ms. The initial synaptic weights ε_{ij} are normally distributed with mean and standard deviation equal to $\varepsilon_M = 0.25$ and 0.02, respectively ($0 \leq \varepsilon_{ij} \leq 2\varepsilon_M$). Then, they are updated according to Eq. (13), where $\varepsilon_{ij} \to \varepsilon_{ij} + 10^{-3}\Delta\varepsilon_{ij}$. The insets in Fig. 1 show the absolute value of the plasticity function, where the red and black lines are the potentiation and depression values, respectively, as a function of Δt_{ij}. The green dashed line in the inset Figures denotes the Δt_{ij} value at wich the curves of potentiation and depression intersect. The inset in Fig. 1(a) shows that for $|\Delta t_{ij}| < 1.8$ms the potentiation of ε_{ij} is bigger than the depression. Whereas in the case of iSTDP (inset in Fig. 1(b)) the potentiation of σ_{ij} is bigger than the depression for $|\Delta t_{ij}| > 9.8$ms.

For the inhibitory iSTDP synapses, the coupling strength σ_{ij} is adjusted based on the equation

$$\Delta\sigma_{ij} = \frac{g_0}{g_{\rm norm}}\alpha^{\beta}|\Delta t_{ij}|\Delta t_{ij}{}^{\beta-1}\exp(-\alpha|\Delta t_{ij}|), \quad (14)$$

where g_0 is the scaling factor accounting for the amount of change in inhibitory conductance induced by the synaptic plasticity rule, and $g_{\rm norm} = \beta^{\beta}\exp(-\beta)$ is the normalizing constant. Figure 1(b) exhibits the result obtained from Eq. (14) for $g_0 = 0.02$, $\beta = 10.0$, $\alpha = 0.94$ if $\Delta t_{ij} > 0$, and for $\alpha = 1.1$ if $\Delta t_{ij} < 0$ (Talathi et al., 2008). As a consequence, $\Delta\sigma_{ij} > 0$ for $\Delta t_{ij} > 0$, and $\Delta\sigma_{ij} < 0$ for $\Delta t_{ij} < 0$. The initial inhibitory synaptic weights σ_{ij} are normally distributed with mean and standard deviation equal to σ_M and 0.02, respectively ($0 \leq \sigma_{ij} \leq 2\sigma_M$). Then, the coupling strengths are updated according to Eq. (14), where $\sigma_{ij} \to \sigma_{ij} + 10^{-3}\Delta\sigma_{ij}$. The updates for ε_{ij} and σ_{ij} are applied for the last postsynaptic spike.

3. Spiking neuron synchronization

To study the effect of plasticity on the neural network, we have calculated the coupling strengths, and used the time-average order-parameter as a probe of spike synchronization, a quantity expressed by

$$R = \frac{1}{t_{\rm final} - t_{\rm initial}}\sum_{t_{\rm initial}}^{t_{\rm final}}\left|\frac{1}{N}\sum_{j=1}^{N}\exp(i\psi_j)\right|, \quad (15)$$

where $t_{\rm final} - t_{\rm initial}$ is the time window for our estimation and the phases are calculated by

$$\psi_j(t) = m + \frac{t - t_{j,m}}{t_{j,m+1} - t_{j,m}}, \quad (16)$$

where $t_{j,m}$ represents the time when a spike m ($m = 0, 1, 2, \ldots$) in neuron j occurs ($t_{j,m} < t < t_{j,m+1}$), with the beginning of each spike being when $V_j > 0$. In synchronous behavior, the order-parameter magnitude approaches unity. In addition, if the spike times are uncorrelated, the order-parameter magnitude is typically small and vanishes for $N \to \infty$. When identical neurons are coupled, the neural network may exhibit complete synchronization among spiking neurons, in other words, all other neurons may present identical time evolution of their action potentials. In this work, we are not considering identical neurons, and as result it is not possible to observe complete synchronization. However, an almost-complete synchronization may be observed.

Figure 2(a) shows the mean order-parameter ($\bar{R}$) that is calculated for different initial conditions, as a function of the inhibitory coupling strength σ_M for a neural network with excitatory and inhibitory synapses, where we consider one case without STDP (black circles) and another with STDP (red triangles). For ε_M equal to 0.25 and varying σ_M, we do not observe a significant alteration of the $\bar{R}$ value without STDP, due to the fact that initially the network has an all-to-all topology. Nevertheless, considering

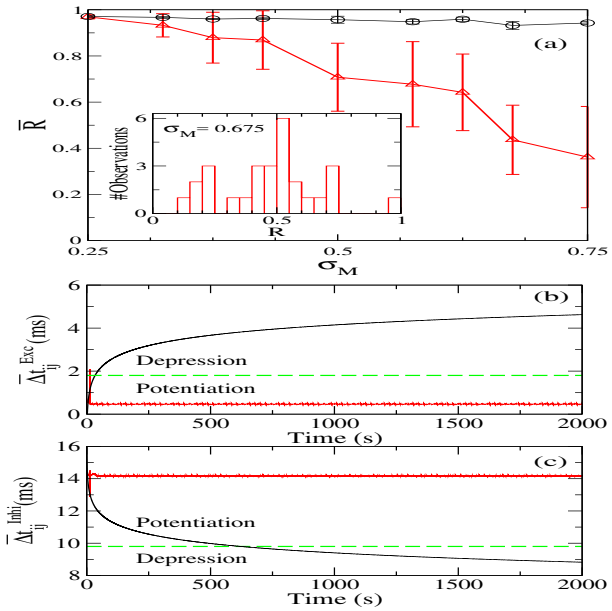

Figure 2: (Color online) (a) Mean order-parameter $\bar{R}$ versus σ_M for $\gamma = 0.0$ and $\varepsilon_M = 0.25$, a result without STDP (black circles) and the other one with STDP (red triangles). The bar is the standard deviation for 30 different initial conditions. In the inset we consider $\sigma_M = 0.675$. Panels (b) and (c) exhibit the time evolution of the average time-difference for excitatory and inhibitory connections, respectively. The black and red lines , for $\sigma_M = 0.675$, correspond to $\bar{R} \approx 0.1$ and $\bar{R} \approx 1$, respectively. The green line represents the separation between potentiation and depression.

STDP we verify that the $\bar{R}$ values decrease with the increase of σ_M and present a large standard deviation. This standard deviation occurs due to the existence of different synchronization states. Then, both the upper border of the inhibitory coupling 2σ and the different initial conditions are important to change the dynamics of the network with STDP and without external perturbation. This is verified by means of the decay of the R values and the large standard deviation bar. In the inset (Fig. 2(a)), we consider $\sigma_M = 0.675$ and calculate the order-parameter for different initial conditions. As a result, we can see a distribution presenting different synchronization states, including desynchronization and synchronization. In Figs. 2(b) and 2(c) we consider $\sigma_M = 0.675$ according to the inset, and calculate the time evolution of the average time-difference for excitatory and inhibitory connections,

$$\bar{\Delta t}_{ij}^{\rm Exc} = \frac{1}{\tau}\sum_{i\neq j}|t_{\rm pre}^{\rm Exc} - t_{\rm pos}|, \quad (17)$$

$$\bar{\Delta t}_{ij}^{\rm Inhib} = \frac{1}{\tau}\sum_{i\neq j}|t_{\rm pre}^{\rm Inhib} - t_{\rm pos}|, \quad (18)$$

respectively, for different configurations of the initial networks and $\tau = 100$ms. The black line shows the case in which the network goes to a desynchronized state ($\bar{R} \approx 0.1$), whereas the red line exhibits the case of a network that presents synchronous behavior ($\bar{R} \approx 1$). In both

cases, we consider the same parameters, except the seed to generate the random distribution of the constant current density I_i. Through Figures 2(b) and 2(c) it is possible to verify why and when the coupling matrix suffer substantial changes. The transition occurs when the black or red curves cross the green line. At this time, depreciation induces weak strength in the coupling matrix, and potentiation induces strong strength.

Figure 3 exhibits the time courses of the mean excitatory (Fig. 3(a)) and inhibitory (Fig. 3(b)) coupling strengths from the multiple coexisting regimes that are shown in Figure 2(a). We see that for $\sigma_M = 0.25$ both $\bar{\varepsilon}_{ij}$ and $\bar{\sigma}_{ij}$ have constant values for the time approximately greater than 700s, and the learning produces a triangular-type connecting matrix (as shown in Fig. 4), meaning that the connections among all neurons become preferentially directed. For $\sigma_M = 0.5$ the $\bar{\varepsilon}_{ij}$ values decrease to approximately 0.15, while $\bar{\sigma}_{ij}$ values oscillate about 0.25, and the coupling matrix becomes partitioned, indicating the existence of larger clusters. Increasing the upper border σ_M to 0.75 both $\bar{\varepsilon}_{ij}$ and $\bar{\sigma}_{ij}$ tend to 0, and the coupling matrix becomes sparse.

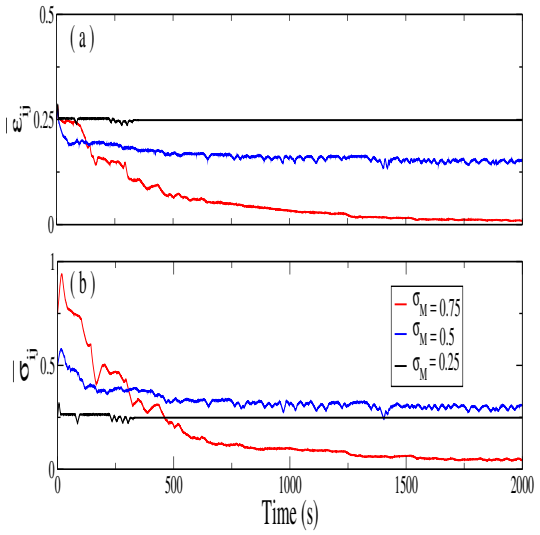

Figure 3: (Color online) Time courses of the mean (a) excitatory and (b) inhibitory coupling strengths from some regimes showed in Figure 2(a).

In Fig. 4, the synaptic weights ε_{ij} and σ_{ij} are encoded in color for $\gamma = 0.0$, $\varepsilon_M = 0.25$, and $\sigma_M = 0.675$, where we choose values of the parameters that provide the cases for (a) $\bar{R} \approx 0.1$ and (b) $\bar{R} \approx 1$ according to the inset in Fig. 2(a). The synaptic weights are suppressed in the desynchronized regime (Fig. 4(a)), and consequently the coupling matrix presents a small number of connections. This behavior can be verified by means of the black lines in Figs. 2(b) and 2(c). In addition, the synaptic weights are potentiated (red lines in Figs. 2(b) and 2(c)) in the synchronized regime (Fig. 4(b)), and the coupling matrix exhibits a triangular shape. We have verified that, in this

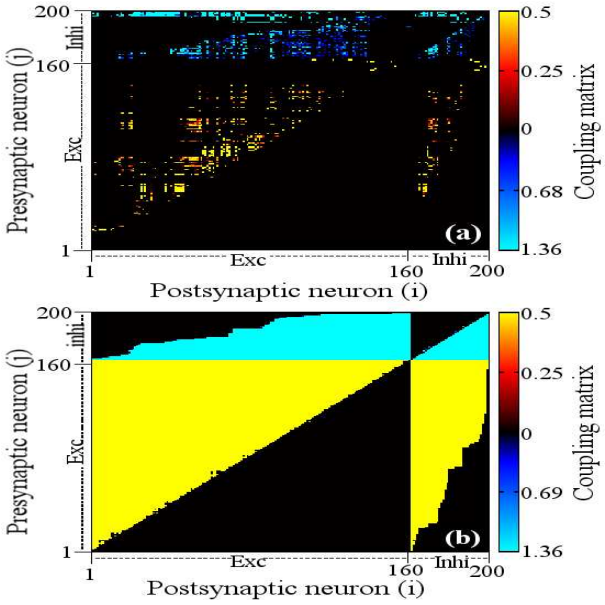

Figure 4: (Color online) Coupling matrix for $\gamma = 0.0$, $\varepsilon_M = 0.25$, and $\sigma_M = 0.675$, where we choose values for parameters to provide the cases for (a) $\bar{R} \approx 0.1$ showing many uncoupled neurons, and (b) $\bar{R} \approx 1$ exhibiting many directed couplings, according to the inset in Fig. 2(a). The synaptic weights are encoded in color, where the maximum value for ε_{ij} (yellow) is 0.5 and the maximum value for σ_{ij} (blue) is 1.36. The neurons are ordered according to $I_i \leq I_j$ for $i < j$.

case, the synchronous behavior has a dependence on the direction of synapses. In other words, when the presynaptic neurons are excitatory the synapses from the high frequency to the low frequency neurons become stronger. When the presynaptic neurons are inhibitory, the synapses from the low frequency to the high frequency neurons become stronger.

Figure 4 shows the final topologies for two networks initially set with a global coupling topologies after being evolved by a STDP proccess. We see that the STDP induces a non-trivial topology in the network resulting in networks sparsely connected, moderately connected (Fig. 4(a)), or densely connected with strong preferential attachment (Fig. 4(b)).

Considering an external perturbation ($\Gamma_i > 0$), we also study the cases without and with plasticity. In the case without STDP, we verify that the mean order-parameter has a small decay when σ_M increases, as shown in Fig. 5(a) with black circles. The red triangles represent the case with STDP, and unlike the case without perturbation (Fig. 2(a)), there is an abrupt transition (blue triangles), due to a first-order transition in the average order parameter. First-order transition is a term that comes from Thermodynamics and here represents a discontinuity of the mean order-parameter function with respect to the inhibitory coupling strength. In this case, the upper border of the inhibitory coupling is relevant to produce alteration in the dynamics, while the different initial con-

ditions are important only at the transition. Based on the results in the inset (Fig. 5(a)), we verify that the network in the transtition can be either in one of the states: (i) high $\bar{R}$ with potentiation of the average-time difference for excitatory and inhibitory connections (red lines in Figs. 5(b) and 5(c)), or (ii) low $\bar{R}$ with excitatory average time-difference in the depression region and inhibitory in the potentiation region (black lines).

The transition from the synchronized to the desynchronized states was reported in studies on how stimulation impact on neurological disorders induced by an abnormal neuronal synchronization (Tass & Majtanik, 2006; Popovych & Tass, 2012). A first order transition was also observed in (Popovych et al., 2013) when the stimulation intensity varies in a neural network with eSTDP. In our simulations, we observe the transition to desynchronization caused by a variation in the inhibitory coupling in neural networks with both eSTDP and iSTDP.

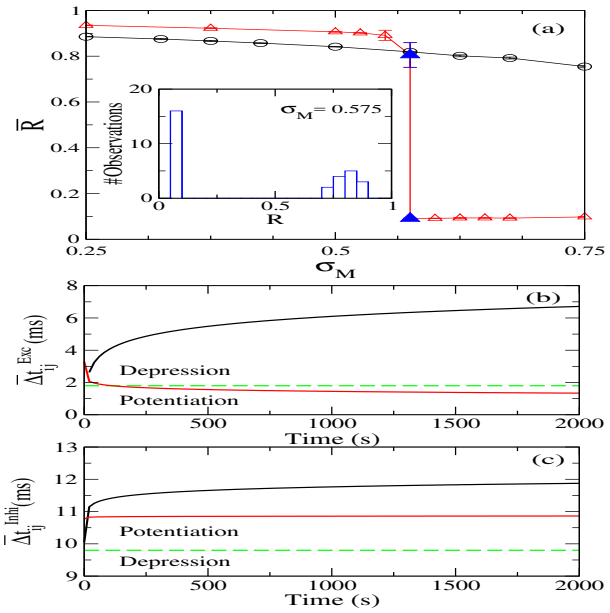

Figure 5: (Color online) (a) Mean order-parameter versus σ_M for $\gamma = 10.0\ \mu\text{A/cm}^2$, $\varepsilon_M = 0.25$, a result without STDP (black circles) and another one with STDP (red triangles). Inset plot for $\sigma_M = 0.575$ (blue triangles) and 30 values of R, where each R is calculated from a different initial configuration. Figures (b) and (c) exhibit the time evolution of the average time-difference for excitatory and inhibitory connections, respectively, where σ_M is equal to 0.575. The black and red lines correspond to $\bar{R} \approx 0.1$ and $\bar{R} \approx 0.8$, respectively. The green dash represents the separation between potentiation and depression.

Figure 6 illustrates the coupling matrix for the two states of the first-order transition. In Fig. 6(a), we can see the coupling configuration that corresponds to high $\bar{R}$. The network presents high connectivity, and for this reason it is possible to observe synchronous behavior. For the case of low $\bar{R}$, we verify that the network has only connections from neurons belonging to the inhibitory population to any other neuron, as shown in Fig. 6(b).

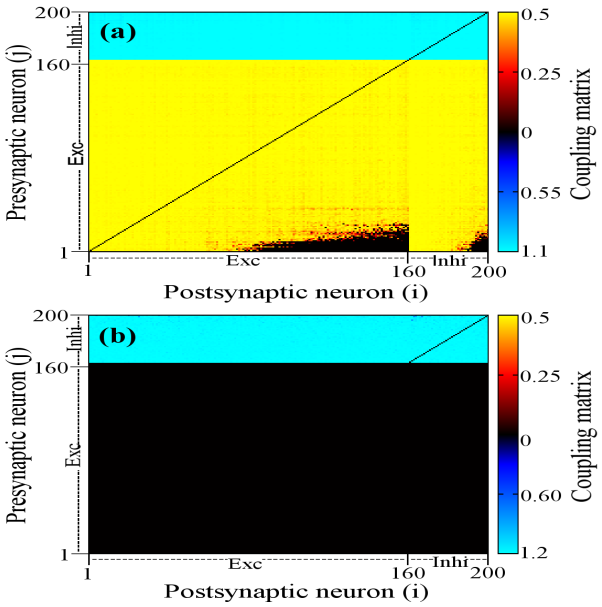

Figure 6: (Color online) Coupling matrix for $\gamma = 10.0\ \mu\text{A/cm}^2$, $\varepsilon_M = 0.25$. (a) $\sigma_M = 0.55$ ($\bar{R} \approx 1$) showing a large quantity of coupled neurons, and (b) $\sigma_M = 0.6$ ($\bar{R} \approx 0.1$) exhibiting connections from inhibithory to excitatory neurons. The synaptic weights are encoded in color, where the maximum value for ε_{ij} (yellow) is 0.5, the maximum value for σ_{ij} (blue) is 1.1 in (a) and 1.2 in (b). The neurons are ordered according to $I_i \leq I_j$ for $i < j$.

4. Conclusion

In conclusion, we have studied the effects of spike timing-dependent plasticity on the synchronous behavior and the evolved connecting topology of neural networks constructed with Hodgkin-Huxley neurons. In our simulations, we considered parameter values for the Hodgkin-Huxley system and STDP according to experimental values found in the neuroscience literature (Bi & Poo, 1998; Haas et al., 2006). Regarding the evolved topology, our main conclusion is that learning under a STDP results in evolved networks that present complex topology. Concerning the dynamic synchronous behavior of the evolved networks, we observe that the studied networks exhibit concurrent synchronous and non synchronous states with characteristics that depend on both the upper border of the inhibitory coupling and the initial conditions. Specifically, we verify that the main role of the inhibitory connections is to produce a delay in the spiking time of the postsynaptic neurons. As a consequence, the increase of the inhibitory coupling strength can suppress synchronous behavior, which contributes to a decrease in the mean order parameter. Moreover, the transition from low to a high synchronous state is smooth by alterations of the inhibitory synapses. When a random external perturbation is introduced in the network, this transition becomes discontinuous, i.e., we observe a first-order transition. Similarly to the non-perturbed network, we also find coexistence of synchronous and non-synchronous neurons in the

perturbed networks.

In future works, we plan to study synchronous states in the brain considering plasticity dynamics in terms of the thresholds for switching on the long-term potentiation and the long-term depression. We also plan to investigate how the final behavior of the network depends on the initial population of excitatory neuron.

Acknowledgments

This study was possible by partial financial support from the following Brazilian government agencies: CNPq, FAPESP (2011/19296-1, 2015/07311-7, 2016/16148-5) and CAPES. AMB, KCI, CGA, and MSB partial support from EPSRC-EP/I032606. We also wish thank Newton Fund and COFAP.

Abarbanel, H. D. I., & Talathi, S. S. (2006). Neural circuitry for recognizing interspike interval sequences. *Physical Review Letters*, 96, 148104.

Abeles, M., Hayon, G., & Lehmann, D. (2004). Modeling compositionality by dynamic binding of synfire chains. *Journal of Computational Neuroscience*, 17, 179-201.

Antonopoulos, C. G., Srivastava, S., Pinto, S. E. S., & Baptista, M. S. (2015). Do brain networks evolve by maximizing their information flow capacity? *PLOS Computational Biology*, 11, 1-29.

Artola, A., Bröcher, S., & Singer, W. (1990). Different voltage-dependent thresholds for inducing long-term depression and long-term potentiation in slices of rat visual cortex *Nature*, 347, 69-72.

Baptista, M. S., Szmoski, R. M., Pereira, R. F., & Pinto, S. E. S. (2016). Chaotic, informational and synchronous behaviour of multiplex networks, *Scientific Reports*, 6, 22617.

Bi, G. Q., & Poo, M. M. (1998). Synaptic modifications in cultured hippocampal neurons: Dependence on spike timing, synaptic strength, and postsynaptic cell type. *The Journal of Neuroscience*, 18, 10464-10472.

Bliss, T.V.P., & Gardner-Medwin, A. R. (1973). Long-lasting potentiation of synaptic transmission in the dentate area of the anaesthetized rabbit following stimulation of the perforant path. *The Journal of Physiology*, 232, 357-374.

Bliss, T.V.P., & Collingridge, G.L. (1993). A synaptic model of memory: long-term potentiation in the hippocampus. *Nature*, 361, 31-39.

Borges, R. R., Borges, F. S., Lameu, E. L., Batista, A. M., Iarosz, K. C., Caldas, I. L., Viana, R. L., & Sanjuán, M. A. F. (2016). Effects of the spike timing-dependent plasticity on the synchronisation in a random Hodgkin-Huxley neuronal network. *Communications in Nonlinear Science and Numerical Simulation*, 34, 12-22.

Brenner, N., Bialek, W., & Van Steveninck, R. R. de R. (2000). Adaptive rescaling maximizes information transmission. *Neuron*, 26, 695-702.

Dayan, E. & Cohen, L. G. (2011). Neuroplasticity subserving motor skill learning. *Neuron*, 72, 443-454.

Destexhe, A., Mainen, Z. F., & Sejnowki, T. J. (1994). An efficient method for computing synaptic conductances based on a kinetic model of receptor binding. *Neural Computation*, 6, 14.

Draganski, B., Gaser, C., Busch, V., Schuierer, G., Bogdahn, U., & May, A. (2004). Neuroplasticity: changes in grey matter induced by training. *Nature*, 427, 311-312.

Fuchs, E., Czéh, B., Kole, M. H. P., Michaelis, T., & Lucassen, P. J. (2004). Alterations of neuroplasticity in depression: the hippocampus and beyond. *European Neuropsychopharmacology*, 14, 481-490.

Gilson, M., Burkitt, A., & Van Hemmen, J. L. (2010). STDP in recurrent neuronal networks. *Frontiers in computational neuroscience*, 4, 1-15.

Golomb, D., & Rinzel, J. (1993). Dynamics of globally coupled inhibitory neurons with heterogeneity. *Physical Review E*, 48, 4810.

Gray, E.G. (1959). Electron microscopy of synaptic contacts on dendrite spines of the cerebral cortex. *Nature*, 6, 1592-1593.

Haas, J. S., Nowotny, T., & Abarbanel, H.D.I. (2006). Spike-timing-dependent plasticity of inhibitory synapses in the entorhinal cortex. *Journal of Neurophysiology*, 96, 3305-3313.

Hammond, C., Bergman, H., & Brown, P. (2007). Pathological synchronization in Parkinson's disease: networks, models and treatments. *Trends in Neurosciences*, 30, 357-364.

Hayon, G., & Lehmann, D. (2005). A model for representing the dynamics of a system of synfire chains. *Journal of Computational Neuroscience*, 18, 41-53.

Hebb, D. O. (1949). *The organization of behavior*. New York: Wiley & Sons.

Hebb, D. O. (1961). *Brain mechanisms and learning*. London, Oxford University Press.

Hodgkin, A. L., & Huxley, A. F. (1952). A quantitative description of membrane current and its application to conduction and excitation in nerve. *The Journal of Physiology*, 11, 500-544.

Izhikevich, E. M. (2004). Which model to use for cortical spiking neurons? *IEEE Transactions on Neural Networks*, 15, 1063.

James, W. (1890). *The principles of psychology*. New York: Henry Holt and Company.

Kalitzin, S., Van Dijk, B. W., & Spekreijse, H. (2000). Self-organized dynamics in plastic neural networks: bistability and coherence. *Biological Cybernetics*, 83, 139-150.

Konorski, J. (1948). *Conditioned reflexes and neuron organization*. Cambridge: Cambridge University Press.

Lashley, K. S. (1923). The behavioristic interpretation of consciousness. *Psychological Bulletin*, 30, 237-272.

Lu, L., Bao, G., Chen, H., Xia, P., Fan, X., Zhang, J., Pei, G., & Ma, L. (2003). Modification of hippocampal neurogenesis and neuroplasticity by social environments. *Experimental Neurology*, 183, 600-609.

Markram, H., Gerstner, W.& Sjostrom , P.J. (2011). A history of spike-timing-dependent plasticity. *Frontiers in synaptic neuroscience*, 3, 1-24.

Markram, H., Gerstner, W.& Sjostrom , P.J. (2012). Spike-timing-dependent plasticity: a comprehensive overview. *Frontiers in synaptic neuroscience*, 4, 1-3.

Noback, C. R., Strominger, N. L., Demarest, R. J., & Ruggiero, D. A. (2005). *The Human Nervous System: Structure and Function* (Sixth ed.). Totowa, NJ: Humana Press.

Popovych, O. V. & Tass, P. A. (2012). Desynchronizing electrical and sensory coordinated reset neuromodulation. *Frontiers in Human Neuroscience*, 6, 1-14.

Popovych, O. V., Yanchuk, S., & Tass, P. A. (2013). Self-organized noise resistance of oscillatory neural networks with spike timing-dependent plasticity. *Scientific Reports*, 3, 2926.

Ramon Y Cajal, S. (1928). *Degeneration and regeneration of the nervous* System. London, Oxford University Press.

Sadeh, S, Clopath, C., & Rotter, S. (2015). Emergence of functional specificity in balanced networks with synaptic plasticity. *PLOS Computational Biology*, 11, 1-27.

Strong, S. P., Koberle, R., Van Steveninck, R. R. de R., & Bialek, W. (1998). Entropy and information in neural spike trains. *Physical Review Letters*, 80, 197-200.

Uhlhaas, P. J., & Singer, W. (2006). Neural synchrony in brain disorders: relevance for cognitive dysfunctions and pathophysiology. *Neuron*, 52, 155-168.

Talathi, S.S., Hwang, D.-U., & Ditto, W. L. (2008). Spike timing dependent plasticity promotes synchrony of inhibitory networks in the presence of heterogeneity. *Journal of Computational Neuroscience*, 25, 262-281.

Tass, P. A. & Majtanik, M. (2006). Long-term anti-kindling effects of desynchronizing brain stimulation: a theoretical study. *Biological Cybernetics*, 94, 58-66.

Wang, Z., Sornborger, A. T. & Tao, L. (2016). Graded, dynamically routable information processing with synfire-gated synfire chains. *PLoS computational biology*, 12, 1-17.